Applied Ergonomics 70 (2018) 68–76

Contents lists available at ScienceDirect

Applied Ergonomics

journal homepage: www.elsevier.com/locate/apergo

Load-embedded inertial measurement unit reveals lifting performance

Aditya Tammana[a], Cody McKay[a], Stephen M. Cain[a], Steven P. Davidson[a], Rachel V. Vitali[a], Lauro Ojeda[a], Leia Stirling[b], Noel C. Perkins[a,*]

[a] Department of Mechanical Engineering, University of Michigan, Ann Arbor, MI, USA
[b] Department of Aeronautics and Astronautics, Massachusetts Institute of Technology, Boston, MA, USA

ARTICLE INFO

Keywords:
Manual load lifting
Performance
Inertial sensors
Biomechanics

ABSTRACT

Manual lifting of loads arises in many occupations as well as in activities of daily living. Prior studies explore lifting biomechanics and conditions implicated in lifting-induced injuries through laboratory-based experimental methods. This study introduces a new measurement method using load-embedded inertial measurement units (IMUs) to evaluate lifting tasks in varied environments outside of the laboratory. An example vertical load lifting task is considered that is included in an outdoor obstacle course. The IMU data, in the form of the load acceleration and angular velocity, is used to estimate load vertical velocity and three lifting performance metrics: the lifting time (speed), power, and motion smoothness. Large qualitative differences in these parameters distinguish exemplar high and low performance trials. These differences are further supported by subsequent statistical analyses of twenty three trials (including a total of 115 total lift/lower cycles) from fourteen healthy participants. Results reveal that lifting time is strongly correlated with lifting power (as expected) but also correlated with motion smoothness. Thus, participants who lift rapidly do so with significantly greater power using motions that minimize motion jerk.

1. Introduction

Manual lifting of loads arises in activities of daily living as well as in the specialized tasks performed by industrial, agricultural and construction workers, athletes, warfighters, emergency responders, and in many other occupations. Such lifting tasks are a well-known risk factor in low back pain. As reviewed in Song et al. (2016), the lifetime prevalence of low back pain in the US alone exceeds 60% (Krismer and van Tulder, 2007) and incurs annual costs exceeding $100 billion (Katz, 2006). Numerous studies explore the underlying mechanisms and lifting conditions implicated in injuries to the lower back; see, for example (Freivalds et al., 1984; Faber et al., 2009; Singh et al., 2014). Multiple biomechanical models of lifting (Freivalds et al., 1984; Singh et al., 2014) explore the lower back and/or shoulder loads during lifting tasks as well as the lifting motions that optimize lifting effort (Song et al., 2015, 2016), together with balance and spine loads (Xiang et al., 2012), and with variable joint stiffness (Hasan, 1986). Among many factors that contribute to injury risk are overexertion and fatigue as revealed by electromyographic data (Shair et al., 2017). Other factors include age and lifting speed, load, range, and technique; see, for example (Albert et al., 1999; Chen, 2000; Kollmitzer et al., 2002; Xiang et al., 2012; Song et al., 2015, 2016; Song and Qu, 2014a; Lee, 2015).

Prior experiments on manual load lifting consider both single hand lifting (Singh et al., 2014; Faber et al., 2009) and two hand lifting (Freivalds et al., 1984; Kollmitzer et al., 2002; Singh et al., 2014; Song and Qu, 2014a; Shair et al., 2017) using a variety of laboratory-based experimental methods. These methods rely principally on video analysis (Freivalds et al., 1984) and optoelectric cameras (Song et al., 2015, 2016; Lee, 2015; Song and Qu, 2014a; Chen, 2000) to deduce body segment pose and kinematics, and force plates to measure ground reactions (Freivalds et al., 1984; Singh et al., 2014; Song et al., 2015, 2016; Song and Qu, 2014a; Kollmitzer et al., 2002). Pertinent to this paper is the study by Song and Qu (2014a) that utilizes an eight-camera optoelectric motion capture system to measure both load and body segment kinematics during two-handed load lifting from floor to shelf heights. The motion capture data, which yield the position, velocity, and acceleration of the load and body segments, reveal significantly different lifting strategies for younger versus older participants. This experiment subsequently informed an optimization study of lifting (Song et al., 2016) that simultaneously considered minimal effort and maximum motion smoothness during lifting. Model results confirm that younger workers tend to minimize effort relative to older workers who tend to maximize load motion smoothness.

While the above laboratory-based methods successfully reveal lifting biomechanics, the conclusions drawn are necessarily somewhat limited by the laboratory conditions employed. Far greater ranges and

* Corresponding author. Department of Mechanical Engineering, University of Michigan, 2350 Hayward St. Ann Arbor, MI 48109-2125, USA.
E-mail address: ncp@umich.edu (N.C. Perkins).

https://doi.org/10.1016/j.apergo.2018.01.014
Received 12 July 2017; Received in revised form 6 December 2017; Accepted 29 January 2018
Available online 21 February 2018
0003-6870/

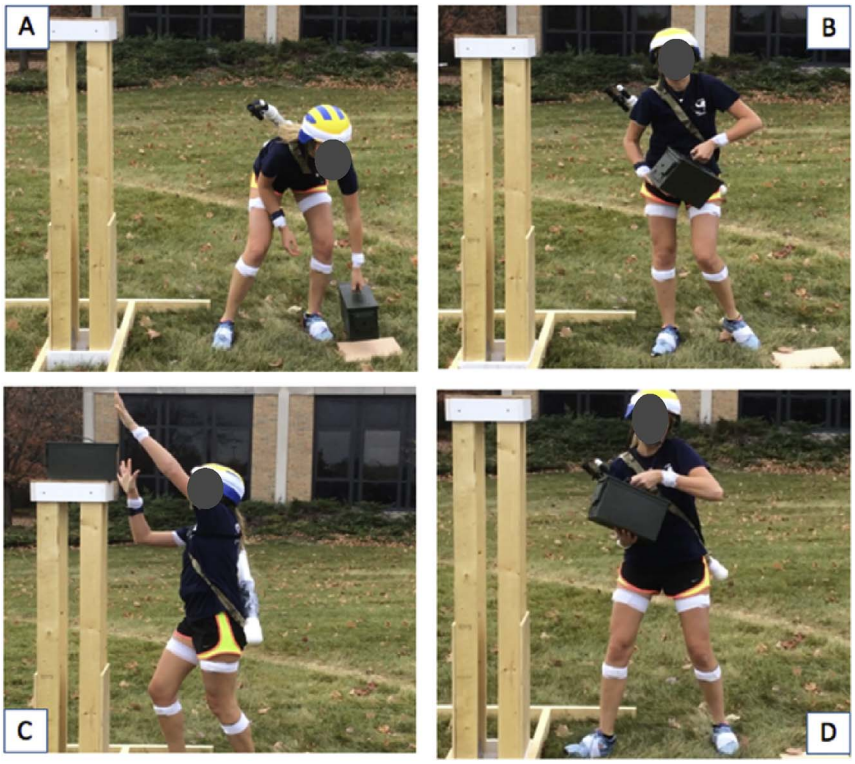

Fig. 1. Vertical load lift obstacle. **A**) Participant picks up the load from the ground (with load at the participant's left side); **B**) rapidly lifts the load upwards; **C**) places the load on stand (momentarily releasing from hands); **D**) rapidly lowers the load downwards and returns it to the ground (momentarily releasing from hands).

variations of lifting conditions exist outside the laboratory, for instance in the home, workplace, training facility, or field of play, where it is difficult if not impossible to use established laboratory measurement methods. A new measurement method, employing load-embedded inertial sensors, holds promise for studying lifting tasks in outdoor and other contextually-relevant environments. The major aims of this paper are to advance the use of miniature inertial measurement units (IMUs) embedded within the load to demonstrate both how lifting can be measured outside of the laboratory and how the measurements can quantify lifting performance.

Miniature embeddable and/or wearable IMUs, which contain MEMS accelerometers and angular rate gyros, are now routinely deployed in a wide range of human motion studies with examples focusing on human mobility (Ojeda and Borenstein, 2007; Rebula et al., 2013; Duong and Suh, 2017), balance training (Lee et al., 2012), human health (Nguyen et al., 2017), athlete performance (King et al., 2008; McGinnis and Perkins, 2012), activity and sleep monitoring (Johannsen et al., 2010; Jean-Louis et al., 2001), and warfighter performance (Davidson et al., 2016; McGinnis et al., 2016; Cain et al., 2016) among others. The use of IMUs for human motion tracking outside of laboratory environments potentially increases the validity of research conclusions. For example, Cain et al. (2016) consider human balance performance in the context of a challenging outdoor balance beam embedded within a larger obstacle course used to assess warfighter performance (Mitchell et al., 2016). Data harvested from an array of body-worn IMUs reveals the fundamental trade-off between speed and stability (balance) for participants traversing the beam with and without added equipment load. Also related to our paper are prior studies that deploy IMUs embedded in hand-held equipment, including athletic equipment (King et al., 2008; McGinnis and Perkins, 2012).

The objective of this paper is to demonstrate how IMUs embedded within loads can reveal lifting performance, including in environments outside the laboratory. To this end, we consider an example load lifting task, embedded in an outdoor obstacle course referred to as the Load Effects Assessment Program (LEAP) (Mitchell et al., 2016). The LEAP is used by military organizations worldwide for several purposes including a means to evaluate the effect of clothing and individual personal equipment on warfighter performance. Performance is assessed on twelve obstacles that include, for example, sprint and agility runs, stair and ladder climbs, window and wall climbs, among others. Important for this study, the LEAP also includes two lifting tasks where a load is lifted with two hands vertically and horizontally. This paper focuses on the vertical lifting task in which participants repeatedly lift and lower a load from ground level to approximately shoulder/head level, akin to prior studies of lifting from floor to shelf heights (see, for example (Song and Qu, 2014a; Song et al., 2016),). We open this paper by describing this vertical lifting task and the theory for using IMU data to quantify lifting performance in terms of three proposed lifting performance metrics; namely, the speed (time), power and smoothness of the lifting motion. We hypothesize that high performance is associated with short lifting times that are enabled by high lifting power and smooth lifting motion. A motivation draws from prior biomechanical models of lifting that associate smoother lifting motions with smaller loads on the lower spine (Freivalds et al., 1984; Hsiang and McGorry, 1997; Song et al., 2016).

2. Methods

2.1. Experimental procedure

Fourteen participants (4 female, 10 male; age = 20.7 ± 1.7 years; body mass = 73.2 ± 11.4 kg; height = 1.77 ± 0.08 m; mean ± standard deviation) for this study were recruited from club sports programs (rugby, triathlon and running) at the University of Michigan. The University of Michigan IRB approved the study, and all participants gave informed consent. Participants wore a military tactical vest, a helmet, and shouldered a mock rifle made of plastic. The participants completed an outdoor obstacle course that was a modified version of the Load Effects Assessment Program (Mitchell et al., 2016) as described above. One obstacle, which is the focus of this paper, was a

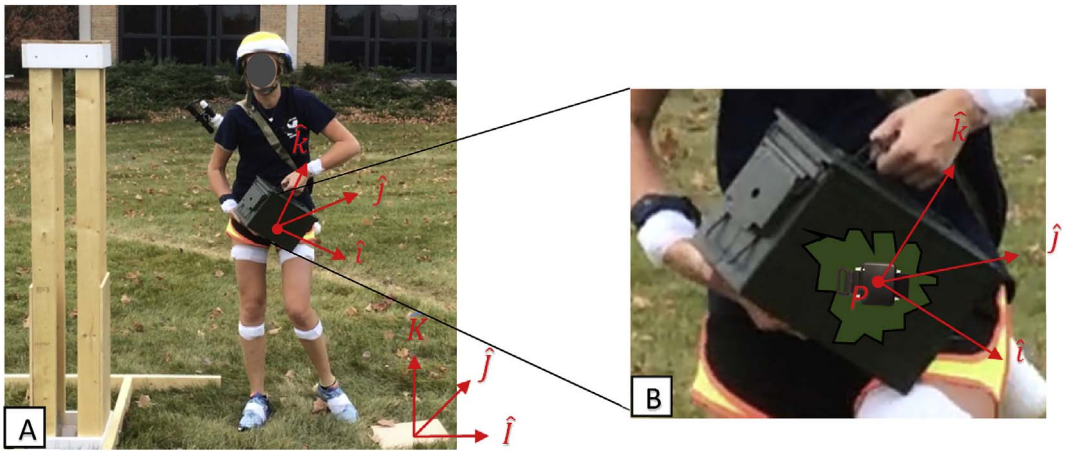

Fig. 2. Field and IMU frames of reference. **A**) The field frame ($\hat{I}$, $\hat{J}$, $\hat{K}$) defines the horizontal ($\hat{I}$ *and* $\hat{J}$) plane of the field and the vertical ($\hat{K}$) direction aligned with gravity. **B**) The IMU frame ($\hat{\imath}$, $\hat{\jmath}$, $\hat{k}$) defines the sense axes of the IMU at the location P of the embedded accelerometer.

vertical load lifting task employing a mock "ammunition can" consisting of a weighted metal box with a handle on the top surface; see Fig. 1.

This vertical load lift required participants to lift the load (mass 13.6 kg) from the ground to the top of a stand (height 1.67 m). In so doing, participants were instructed to lift the load as rapidly as possible from the ground, place it on top of the stand, momentarily release their hand(s) from the load, and then rapidly lower the load back to the ground, and momentarily release their grasp again; refer to Fig. 1. Participants repeated this rapid lift/lower cycle five times with the load positioned to their right side and then repeated the experiment with the load positioned to their left side (as is the case shown in Fig. 1) which is a commonly used procedure in the LEAP.

Performance on this lifting task was evaluated using data harvested from an IMU embedded within the load (i.e. within the can); refer to Fig. 2B. The IMU (Opal, APDM Wearable Technologies, Inc., Portland OR) measured the three-axis acceleration (± 6 g range at the location of an internal accelerometer), the three-axis angular rate of the load (± 2000 deg/s range via an internal angular rate gyro), and the local magnetic field (± 6 Gauss via an internal magnetometer). In addition, the manufacturer's software (Motion Studio, APDM) outputs the quaternions that define the orientation of the IMU with respect to an inertial frame of reference as further described below. These quantities were sampled at 128 Hz and stored to internal memory for subsequent downloading and data reduction. Collectively, the data from the load-embedded IMU was used to estimate the motion of the load as well as the force of the participant's hand(s) imparted on the load as described next. The estimated motion and force variables provide a rich description of lifting performance.

2.2. IMU data reduction for load motion and lifting performance

The motion of the load reduces to describing the motion of a frame of reference fixed to the IMU. This frame of reference, illustrated by ($\hat{\imath}$, $\hat{\jmath}$, $\hat{k}$) in Fig. 2, represents the three mutually orthogonal sense axes of the inertial sensor located at point *P* embedded within the load. This IMU frame of reference differs from the (stationary) inertial frame of the field represented by ($\hat{I}$, $\hat{J}$, $\hat{K}$) in Fig. 2. The unit vectors $\hat{I}$ and $\hat{J}$ span the (horizontal) plane of the field while gravity acts along the $-\hat{K}$ direction. The direction cosine matrix *c(t)* relates the orientation of the IMU frame to the field frame as a function of time as the load moves. In particular,

$$\begin{pmatrix} \hat{\imath} \\ \hat{\jmath} \\ \hat{k} \end{pmatrix} = \mathrm{c(t)} \begin{pmatrix} \hat{I} \\ \hat{J} \\ \hat{K} \end{pmatrix} \tag{1}$$

This direction cosine matrix *c(t)* is required in the following analysis. We outline this analysis in sufficient detail below to allow it to be reduced to code in any programming language starting from the data that represents the output from the IMU.

The software (Motion Studio) provided by the IMU manufacturer (APDM Wearable Technologies, Inc., Portland OR) provides two outputs that are employed in this study. The first is the acceleration sampled by the on-board accelerometer represented by three components (a_x, a_y, a_z) measured along the aforementioned IMU sense axes by ($\hat{\imath}$, $\hat{\jmath}$, $\hat{k}$). The second are the quaternions (q_0, $q_1 q_2$, q_3) that define the orientation of the IMU sense axes relative to the field frame. The quaternions, which are estimated from sensor fusion algorithms proprietary to the manufacturer, are used in our analysis to construct the above direction cosine matrix per

$$c(t) = \begin{bmatrix} (q_0^2 + q_1^2 - q_2^2 - q_3^2) & 2(q_1 q_2 + q_0 q_3) & 2(q_1 q_3 - q_0 q_2) \\ 2(q_1 q_2 - q_0 q_3) & (q_0^2 - q_1^2 + q_2^2 - q_3^2) & 2(q_2 q_3 + q_0 q_1) \\ 2(q_1 q_3 + q_0 q_2) & 2(q_2 q_3 - q_0 q_1) & (q_0^2 - q_1^2 - q_2^2 + q_3^2) \end{bmatrix} \tag{2}$$

The IMU data reduction begins with computing the acceleration of the load along the vertical ($\hat{K}$) direction so that one can also estimate the vertical velocity of the load. To this end, the 3-axis acceleration measured by the IMU

$$\vec{a}_{measured} = a_x \hat{\imath} + a_y \hat{\jmath} + a_z \hat{k} \tag{3}$$

detects the acceleration of point *P* ($\vec{a}_P$) relative to the IMU frame as well as the superimposed acceleration due to gravity $g\hat{K}$. That is,

$$\vec{a}_{measured} = \vec{a}_P + g\hat{K} \tag{4}$$

We desire $\vec{a}_P$ expressed in components in the field frame per

$$\vec{a}_P = A_x \hat{I} + A_y \hat{J} + A_z \hat{K} \tag{5}$$

Using (1)–(5), the field frame components of $\vec{a}_P$ are readily computed from

$$\begin{bmatrix} A_x \\ A_y \\ A_z \end{bmatrix} = c^T \begin{bmatrix} a_x \\ a_y \\ a_z \end{bmatrix} - \begin{bmatrix} 0 \\ 0 \\ g \end{bmatrix} \tag{6}$$

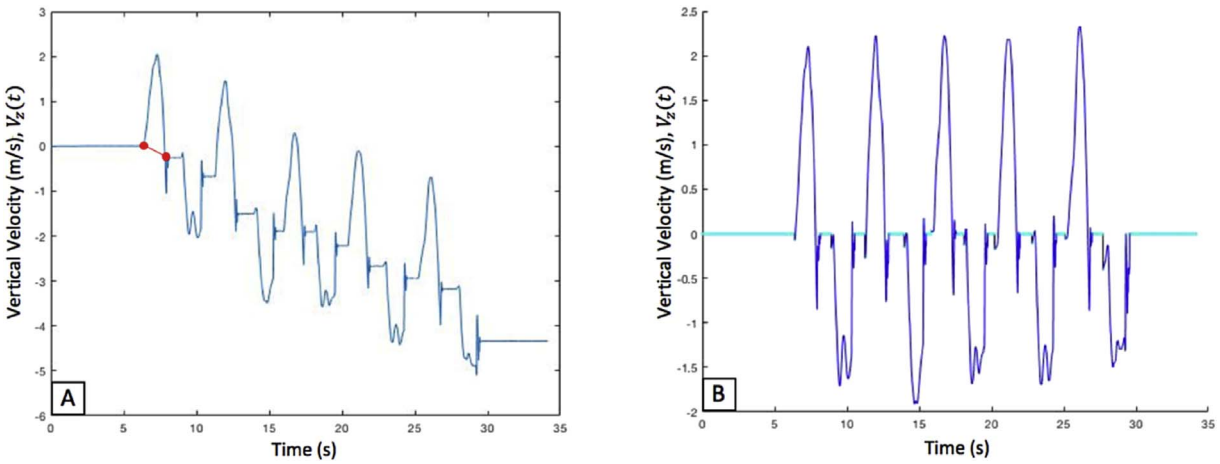

Fig. 3. Estimating the vertical velocity of the load during the lift/lower cycles. **A)** Example velocity profile over five lift/low cycles per Equation (7) illustrates obvious slowly varying drift error. Drift error model is estimated by straight line (red) segments for each lift and lower. **B)** Resulting drift corrected velocity estimate with still periods on the ground and the stand enforced. Locations of zero velocity update points are indicated by cyan dots. (For interpretation of the references to colour in this figure legend, the reader is referred to the Web version of this article.)

where c^T denotes the transpose of the direction cosine matrix (2) and in which A_z(t) is the desired vertical ($\hat{K}$) acceleration component of the load.

Next, we estimate the vertical velocity of the load by numerical integration of A_z(t) per

$$\hat{V}_z(t) = \int_{t_1}^{t} A_z(t)dt + \hat{V}_z(t_1) \tag{7}$$

where $\hat{V}_z(t_1)$ denotes the estimated initial vertical velocity of the load at the start of a lift or lower cycle (which is expected to be zero). Fig. 3A illustrates the result of this computation for an example trial composed of five consecutive lift/lower cycles during the lift/lower time interval $t_1 \approx 6.5 \leq t \leq 29 \approx t_2$ seconds. This result shows an obvious (slowly varying) velocity drift error that is a well-known limitation of estimates based on inertial sensor data as described in the literature on inertial navigation (Savage, 2002; Rogers, 2003). Fortunately, in this application, the drift error is readily estimated and then corrected by simple adaptation of the zero velocity update strategy (ZUPT strategy) developed in the context of studies employing foot-mounted IMUs to estimate three-dimensional trajectories of feet for human subjects while walking (Ojeda and Borenstein, 2007). Specifically, we use the ZUPT strategy to calculate the trajectory of the load between consecutive times of zero velocity (i.e. when the load is on the ground or on the stand) which is analogous to the ZUPT strategy used in (Ojeda and Borenstein, 2007) for estimating the trajectory of the foot between times of zero foot velocity (i.e. when the foot is momentarily at rest on the ground). The details of this approach are as follows.

First, we observe that the load motion over a lift cycle and a lower cycle must begin and end with the load at rest. Thus, the vertical velocity must be zero at the start and at the end of each lift cycle and lower cycle. This requirement is enforced by assuming a linear drift error having slope

$$\alpha = \frac{\hat{V}_z(t_2) - \hat{V}_z(t_1)}{t_2 - t_1} \tag{8}$$

where t_1 and t_2 now denote the start and end of a lift (or lower), respectively. Fig. 3A illustrates an example of this linear drift error estimate for the first lift as seen by the superimposed red line segment. The times t_1 and t_2 for this linear drift error estimate are illustrated by the red dots in this figure. The drift-corrected estimate of the vertical load velocity $V_z(t)$ follows by subtracting this red line segment from the previous vertical velocity estimate per

$$V_z(t) = \hat{V}_z(t) - (\hat{V}_z(t_1) + \alpha t) \text{ on the interval } t_1 \leq t \leq t_2 \tag{9}$$

where, in addition, we require that the load have zero velocity during any "still period" when it is in (momentary) contact with either the ground or the stand. Fig. 3B illustrates the associated drift-corrected result for this example where the five lift/lower cycles are readily observable.

We offer the following additional comments about using load-embedded IMUs for measuring lifting using the method outlined above. The selected load-embedded IMU allows for data collection over extended periods of time on a fully charged battery. In particular, data can be wirelessly transmitted (for up to 8 h) for continuously employing the methods above, or it can be logged (for up to 16 h) for batch processing using the methods above. Thus, either mode enables the collection and the analysis of lifting data over extended periods of time and far greater than the periods of time required in our example experiments enabling the method to be applied in other contextually-relevant settings. Importantly, the drift correction is only needed for the short time intervals when the load is actually being lifted. Thus, tasks in which the load remains at rest for potentially long durations pose no further challenge than when the load remains at rest only briefly/intermittently as in the experiment considered herein. However, the drift correction method does assume that the lifting takes place over a reasonably short period of time for which the linear drift model above remains a good fit (say, lifts occurring within 1 min or less).

Recall that study participants were instructed to lift and lower the load as rapidly as possible. Thus, high performance is associated with short lift and lower times. In addition, we hypothesize that high performance will also correlate with large power exerted by the hand during lifting and lowering, and with smooth lifting and lowering motions. Note that biomechanical models of lifting have explored the role of load motion smoothness (Hsiang and McGorry, 1997; Song et al., 2015, 2016). To these ends, the IMU-derived vertical velocity above is subsequently used to estimate: 1) the lift/lower times, 2) the power exerted by the hand, and 3) the motion smoothness as described next.

Fig. 4 illustrates the vertical velocity of the load over a single example lift/lower cycle where critical timing events are annotated. These events include the lift and lower times, the momentary periods when the load is resting on the stand and the ground, the instants of initial impact of the load on the stand and the ground, and the short periods when the load rattles on the stand and ground before coming to rest. From this decomposition of events, we report the lift and lower times as the time interval when the load is actively being lifted or lowered by the participant as illustrated in Fig. 4. Note specifically that the lift and lower times exclude the short periods when the load is rattling or resting on the stand or the ground.

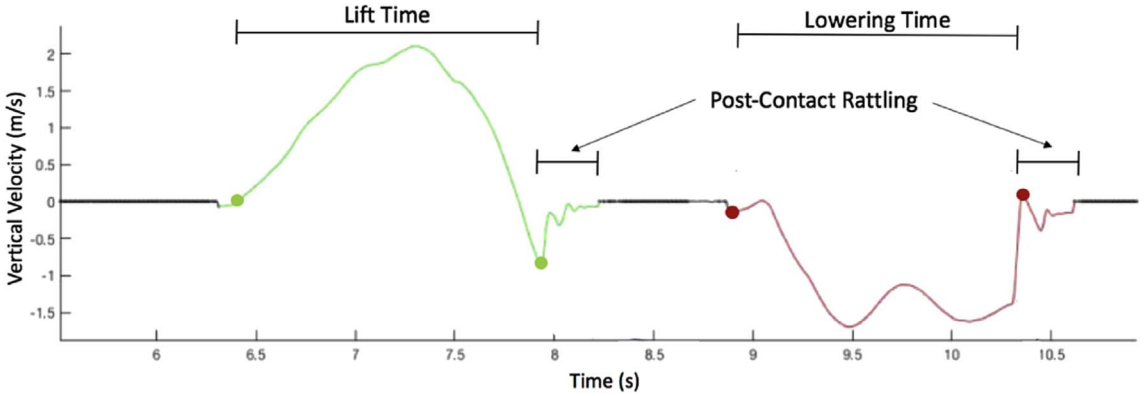

Fig. 4. Vertical (drift corrected) load velocity of an example lift and lower cycle. Shown are the short periods (grey) when the load remains momentarily still on the stand and the ground, the time of initial impact with the stand and the ground, and the brief settling periods where the load is in rattling contact with the stand and the ground.

An estimate of the power exerted by the hand while vertically lifting and lowering the load follows from

$$P(t) = m[A_z(t) + g]V_z(t) \tag{10}$$

where m is the mass of the load and $m(A_z(t) + g)$ is an estimate of the vertical force applied by the participant's hand. In the following, we report the average power delivered during the lifting phases and the lowering phases per

$$P_{average} = \frac{1}{t_{phase}} \int_0^{t_{phase}} P(t)dt \tag{11}$$

where t_{phase} denotes the measured lift time or lower time defined above. Following from the example illustrated in Fig. 4, the associated power and average power for one lift and lower cycle is illustrated in Fig. 5.

We propose a measure of motion smoothness to further evaluate lifting task performance drawing from the extensive literature on both unrestrained and end-point constrained human movement; see for example (Flash and Hogan, 1985; Atkeson and Hollerbach, 1985; Flash, 1987; Uno et al., 1989; Breteler et al., 2001), as well as prior biomechanical simulations of optimum lifting planning (Hsiang and McGorry, 1997; Song et al., 2015, 2016). One such measure follows from comparing the (drift corrected) velocity profile $V_z(t)$ during lifting and lowering phases to the optimum velocity profile that minimizes motion jerk. Adapting results from (Flash and Hogan, 1985), the optimum (minimum jerk) velocity profile for lifting (or lowering) the load over the height h and over lift (or lower) phase time t_{phase} is

$$V_{opt}(t) = \pm \frac{30ht^2(t_{phase} - t)^2}{t_{phase}^5} \tag{12}$$

where the positive sign is chosen for a lifting phase and the negative sign is chosen for a lowering phase. Thus, the optimum velocity profile is determined by the lift (or lower) phase time (t_{phase}) naturally chosen by the participant. Fig. 6 compares this optimum velocity profile to a measured velocity profile during the lift phase previously illustrated in Fig. 4. The difference between these two velocity profiles is one measure of smoothness. In particular, we introduce the normalized RMS difference between $V_z(t)$ and $V_{opt}(t)$ as a motion smoothness (SM) measure:

$$SM = \left[\sqrt{\frac{\int_0^{t_{phase}} [V_z(t) - V_{opt}(t)]^2 dt}{t_{phase}}} \Big/ \sqrt{\frac{\int_0^{t_{phase}} [V_{opt}(t)]^2 dt}{t_{phase}}} \right] X\ 100\% \tag{13}$$

where smaller values of SM designate smoother motions (i.e., motions having less jerk).

We open by comparing the performance metrics for an exemplar high performance trial and an exemplar low performance trial to illustrate major qualitative differences in performance. We began by considering possible differences in performance between lifting from the right to the left side versus lifting from the left to the right side. Analysis of the pooled data (right to left versus left to right) revealed no significant differences between motion directionality in any of the three performance metrics (lift/lowing time, power and smoothness) using signed rank Wilcoxon tests ($p > 0.05$ for all three tests). As no differences were detected between right to left and left to right, we do not

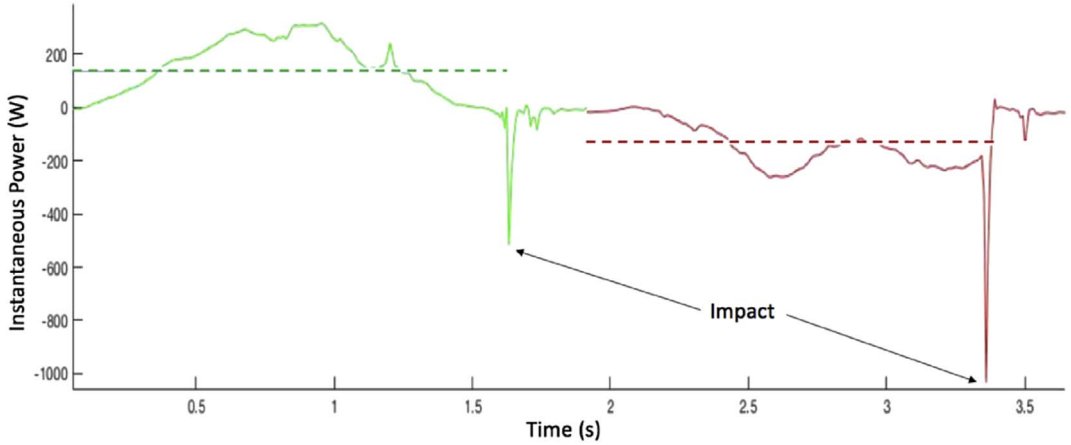

Fig. 5. The estimated instantaneous power (solid curves) and average power (dashed lines) exerted by the hand during one lifting phase (green) and lowering phase (red) for the example of Fig. 4. (For interpretation of the references to colour in this figure legend, the reader is referred to the Web version of this article.)

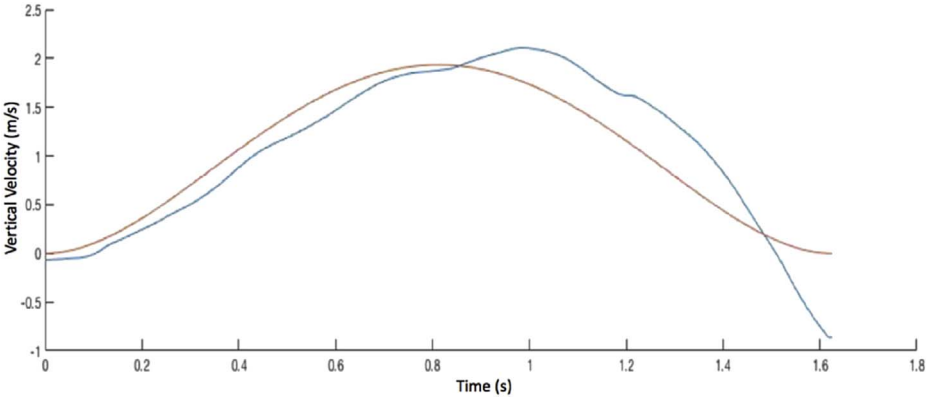

Fig. 6. Motion smoothness. The participant's (drift corrected) velocity profile $V_z(t)$ during an example lift phase (blue) is compared to the optimum velocity profile (red) that minimizes jerk over the same lifting phase time ($t_{phase} \approx 1.63$ seconds). (For interpretation of the references to colour in this figure legend, the reader is referred to the Web version of this article.)

distinguish directionality of trials for the remaining tests. We also examine and report below possible linear relations between the three performance metrics by fitting a linear regression and estimating the Pearson product-moment correlation (r). The assumptions of the linear regressions were assessed by examining if the residuals were normally distributed with constant variance.

3. Results and discussion

As described above, each of the fourteen participants completed the lifting task twice, once starting with the load on the right side of the body (five lift/lower cycles to define one trial) and once again with the load starting on the left side (another five lift/lower cycles to define another trial). Of the resulting 28 trials, five were unusable because the participants did not conform to instructions, yielding a total of N = 23 trials incorporating a total of 115 lift/lower cycles for inclusion in the study. Example reasons for excluding trials included the inadvertent dropping or kicking of the load and not fully releasing hands from the load when the load is placed on the platform or ground. We open this section by highlighting differences in performance with high performance defined by short lift/lower times.

3.1. Comparison of two example trials: exemplar high and low performance trials

Recall that we asked participants to complete the task as quickly as possible. Consequently, we assess performance from the mean time a subject takes to lift the load in each trial with a trial being the five consecutive lift/lowering cycles from one side (right or left). For illustrative purposes, we select a representative trial from a subject with one of the fastest lift times (the exemplar high performance trial) and a trial from a subject with one of the slowest lift times (the exemplar low performance trial). Doing so enables one to quickly understand major qualitative differences in performance as discussed next.

Fig. 7 illustrates results for the exemplar high performance trial (average lift time and lower time = 1.56 s and 1.43 s, respectively). Shown in Fig. 7A are the mean, minimum and maximum vertical velocity profiles (blue) including lifting and lowering phases averaged across all five lift/lower cycles. Also shown is the associated velocity profile (red) for V_{opt} that minimizes motion jerk, per Eqn. (12). The velocity profiles are normalized by the maximum value of V_{opt} and they are plotted versus normalized time t/t_{cycle} where t_{cycle} denotes the mean time to complete a lift/lower cycle. (Thus, t/t_{cycle} denotes the fraction of the cycle time). Fig. 7B reports the corresponding average, minimum, and maximum power over all five lift/lower cycles. Fig. 8 summarizes the analogous results for the exemplar low performance trial (average lift time and lower time = 3.24 s and 1.79 s, respectively over all five lift/lower cycles).

Inspection of Figs. 7 and 8 reveals clear qualitative distinctions between the exemplar high and low performance trials. First, note that the lifting phase illustrated in Fig. 8A exhibits three pronounced local maxima compared to the single local maxima exhibited in Fig. 7A. This major difference underlies that the participant was unable to smoothly lift the load from the ground to the stand in one motion. Instead the participant used a three-stage lifting technique whereby the load was first lifted to approximately waist level, then chest level, then finally to the level of the stand. This three-stage lift takes considerably longer time (108% longer relative to mean lift time of the exemplar high performance trial) and is also considerably less smooth when compared to the optimal (minimal jerk) velocity profile. By contrast, the lowering phase of the low performance trial more closely resembles that for the high performance trial including the lower time (only 25% longer relative to the mean lower time for the exemplar high performance trial). As a result, the entire lift/lower cycle for the low performance trial exhibits significant imbalance with the lifting phase consuming considerably more cycle time compared the balanced lift and lower phases exhibited in the high performance trial. These qualitative differences are also apparent in the instantaneous power illustrated in Figs. 7B and 8B. In particular, the power for the exemplar high performance trial exhibits a single (large) maximum half way through the lifting phase. By contrast, the power for the exemplar low performance trial exhibits three local (small) maxima that again underlie the three-stage lifting technique. Table 1 summarizes the computed timing, power and smoothness metrics for the exemplar high and low performance trials. Reported are the mean (and standard deviation) for each metric for the two selected trials.

Table 2 reports the mean and standard deviation for each performance metric across all 23 trials included in the study. The trial means and standard deviations for lift time, lift power and lift smoothness (SM) are computed across the five consecutive lifts that constitute a trial. Similarly, the trial means and standard deviations for lower time, lower power and lower smoothness (SM) are computed across the five consecutive lowers that constitute a trial. Note that variation in each performance metric is markedly greater for the lift phase compared to the lower phase. In particular, the variation in the lift time is over three times that of the lower time; the variation in the lift power is over two times that of the lower power; and the variation in the lift smoothness is over three times that of the lower smoothness. Thus, while the lift phase readily distinguishes performance, the lower phase may not. In essence, all participants lower the load far more consistently than they raise the load, a conclusion that is also apparent upon re-inspection of the velocity profiles in Figs. 7A and 8A for the exemplar high and low performance trials. These profiles reveal that the participants exploit gravity to largely drop the load at the start of the lowering phase and then arrest the fall of the load during the second half of the lowering phase.

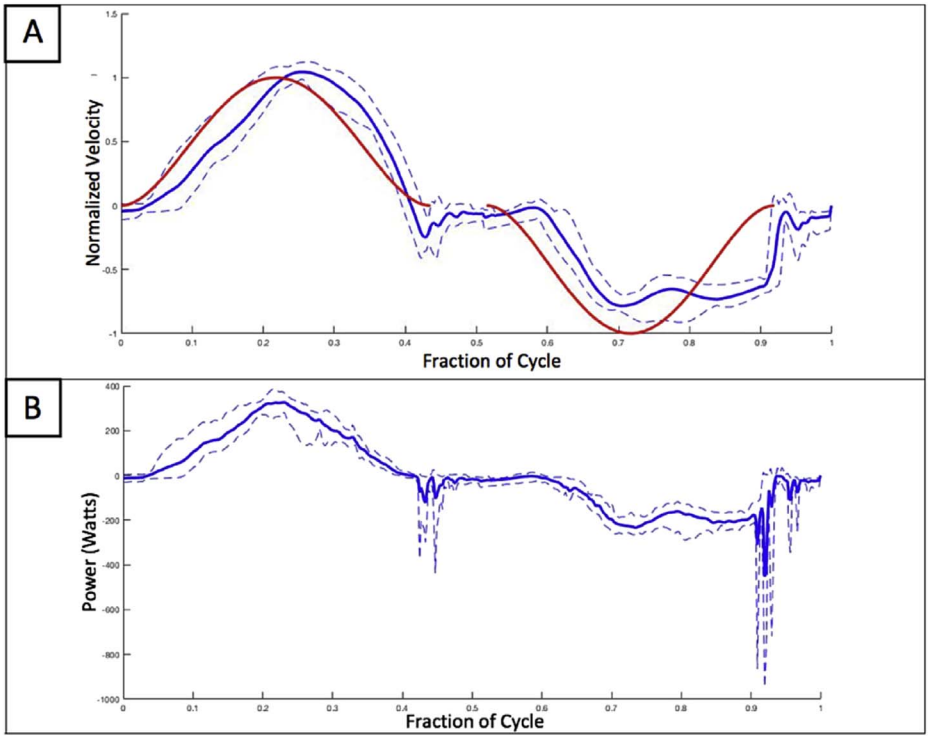

Fig. 7. Results for an exemplar high performance trial. **A)** Mean (blue), minimum (dashed blue) and maximum (dashed blue) normalized vertical velocity over all five lift/lower cycles as functions of normalized time. Associated optimal velocity profile (red) that minimizes motion jerk. **B)** Mean (blue), minimum (dashed blue) and maximum (dashed blue) power over all five lift/lower cycles. (For interpretation of the references to colour in this figure legend, the reader is referred to the Web version of this article.)

To test our original hypotheses, we consider next possible correlations among the three performance metrics for the lift phase; namely the participant mean lift time, mean lift power, and mean lift smoothness. Fig. 9 includes pairwise comparisons of lift power versus lift smoothness (Fig. 9A), lift power versus lift time (Fig. 9B), and lift smoothness versus lift time (Fig. 9C). Fig. 9A reveals a moderate-to-high negative correlation ($r = -0.841$) between lift power and lift SM with trials achieving greater power also exhibiting greater motion smoothness (recall, velocity profiles closer to the optimum yield smaller motion smoothness values SM per Eqn. (12)). A high negative ($r = -0.896$) correlation is observable in Fig. 9B which confirms that shorter lift times require greater lift power. This result is expected since, regardless of lift time, all participants lift the load the same height and thus exert the same change in gravitational potential energy during the lift phase. Changing that energy in shorter time derives from greater lift power. We also observe that the slope of the line may be affected by an apparent outlier (with lift time of approximately 4.5 s). Thus, while the data meet the underlying assumptions for a linear regression, the

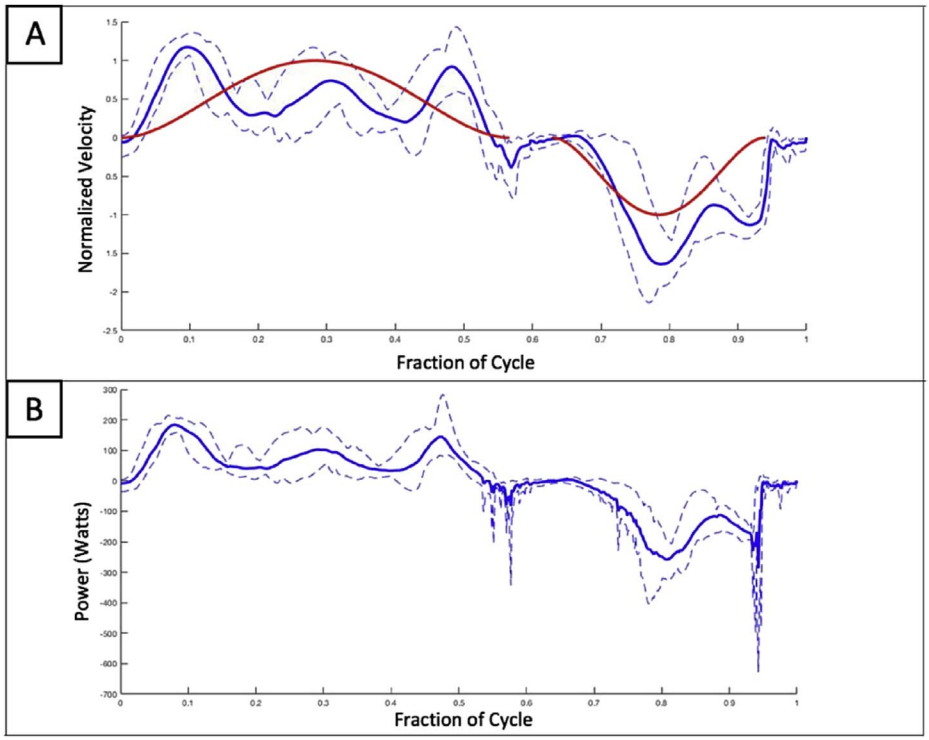

Fig. 8. Results for an exemplar low performance trial. **A)** Mean (blue), minimum (dashed blue) and maximum (dashed blue) normalized vertical velocity over all five lift/lower cycles as functions of normalized time. Associated optimal velocity profile (red) that minimizes motion jerk. **B)** Mean (blue), minimum (dashed blue) and maximum (dashed blue) power over all five lift/lower cycles. (For interpretation of the references to colour in this figure legend, the reader is referred to the Web version of this article.)

Table 1
Performance results for the exemplar high performance trial and low performance trial (5 lifts and 5 lowers each) illustrated in Figs. 7 and 8. Mean (and standard deviation) across all five cycles for the lifts and all five cycles for lowers are reported for lift and lower time, lift and lower power, and lift and lower smoothness (SM).

Exemplar Trial	Lift Time mean (sd) seconds	Lower Time mean (sd) seconds	Lift Power mean (sd) Watts	Lower Power mean (sd) Watts	Lift *SM* mean (sd) %	Lower *SM* mean (sd) %
High Performance	1.56 (.08)	1.43 (.09)	145.5 (14.1)	−139.8 (26.5)	28.7 (10.9)	45.9 (3.5)
Low Performance	3.24 (.42)	1.79 (.12)	71.4 (17.1)	−117.0 (19.9)	86.7 (20.0)	49.9 (7.7)

Table 2
Pooled results for 23 trials (115 lifts and 115 lowers). Mean and standard deviation (and as percent of mean) for six performance metrics including lift and lower time, lift and lower power, and lift and lower smoothness (SM).

Performance Metric	mean	sd (% of mean)
Lift Time (seconds)	2.02	0.77 (38.0%)
Lower Time (seconds)	1.52	0.19 (12.4%)
Lift Power (Watts)	126.90	32.04 (25.3%)
Lower Power (Watts)	−131.59	14.61 (11.1%)
Lift *SM (%)*	52.51	31.11 (59.2%)
Lower *SM (%)*	48.52	9.11 (18.8%)

apparent outlier was included and affects the estimation of the slope. More data would be needed to determine any nonlinear trends. Fig. 9C reveals a high positive correlation ($r = 0.904$) between lift SM and lift time with shorter (faster) lifts being smoother (i.e., correlated with smaller values of SM). This result was not anticipated given that one might be able to lift the load slowly and also smoothly (minimizing jerk). However, the experiment may be biased to exhibit smooth lifting due to the overwhelmingly large inertia (13.6 kg) of the load. Greater jerk may arise with smaller loads at the expense of faster lift time and possibly lead to greater variation in smoothness.

4. Study extensions and limitations

While the focus of this study is to demonstrate how IMUs embedded within loads can reveal lifting performance (as defined by short lift times in the example obstacle course), the method may also have value in future studies of lifting biomechanics and injury potential. In particular, prior studies reveal that faster lifting (also referred to as loading rate or load lifting duration) is associated with larger loads on the lower spine (Freivalds et al., 1984; Singh et al., 2014; Maduri et al., 2008; Song and Qu, 2014b; Song et al., 2016). In addition, smoother (less jerky) lifting motions are associated with smaller loads on the lower spine (Freivalds et al., 1984; Hsiang and McGorry, 1997; Song et al., 2016). Thus, while this study is motivated by the need to assess lifting performance in an outdoor obstacle course, the methods developed may well have broader use for understanding lifting biomechanics and injury potential in other contextually-relevant settings (i.e., outside the laboratory).

The specific findings of this study are necessarily limited by the chosen experimental conditions which were pertinent to the LEAP. These conditions included a relatively large load (13.6 kg), a relatively large lift height (1.67 m), and relatively quick lifts (participants instructed to complete the lifts as rapidly as possible). In addition, the participants were drawn solely from a young (age = 20.7 ± 1.7 years), healthy and athletic population.

5. Summary and conclusions

This paper introduces the use of load-embedded IMU technology to

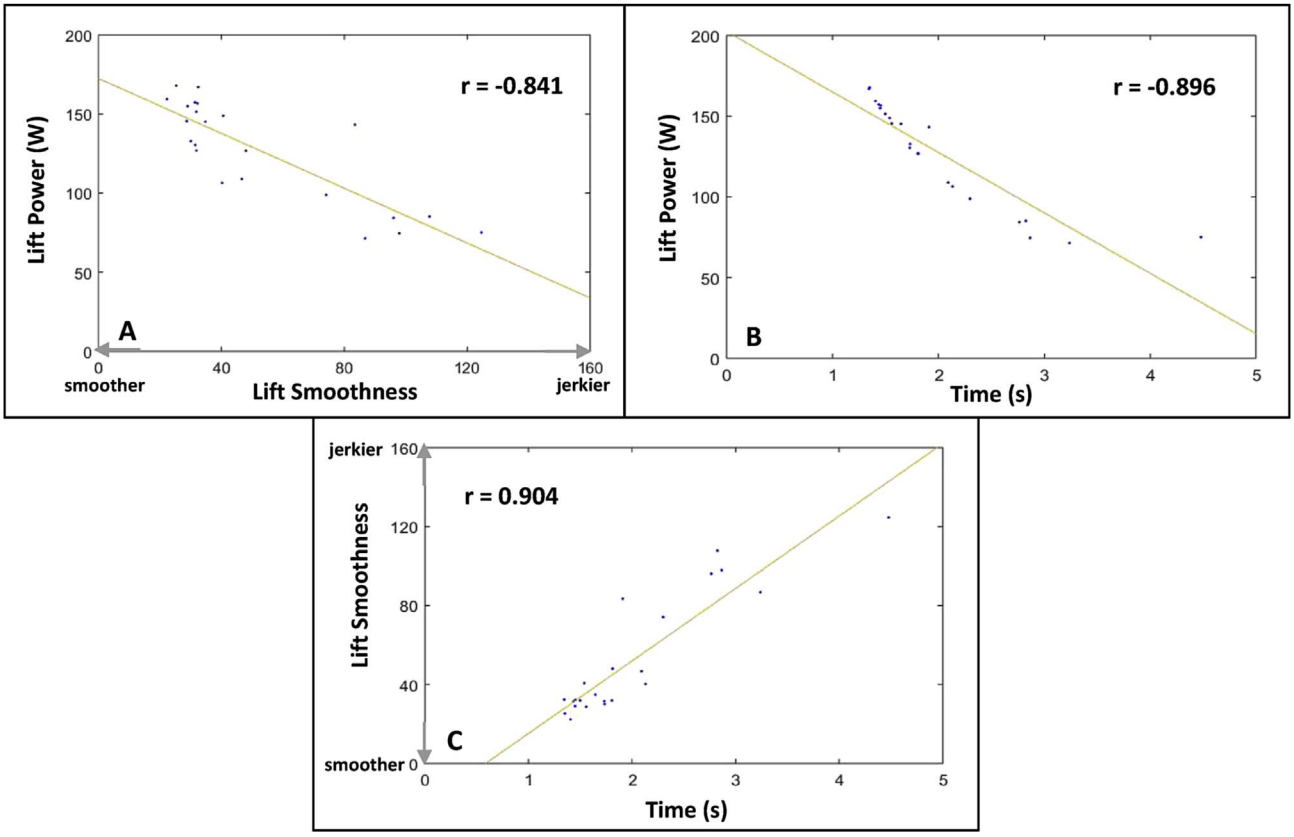

Fig. 9. A: Lift power versus lift smoothness and best fit line (amber); **B:** Lift power versus lift time and best fit line (amber); **C:** Lift smoothness versus lift time and best fit line (amber).

measure and to quantify lifting performance in environments outside the laboratory. The task considered requires repeatedly lifting and lowering a load (13.6 kg) vertically a prescribed height. This lifting task represents one obstacle embedded in a larger obstacle course (Load Effects Assessment Program) used to assess warfighter performance (Mitchell et al., 2016). The angular velocity and acceleration data harvested from the embedded IMU yields estimates of the vertical acceleration and velocity of the load for subsequent performance analysis. Three metrics of performance are proposed; namely, the time, power, and motion smoothness of the lifting and lowering phases of the task. These performance metrics are studied using data from a population of fourteen healthy participants executing a total of 23 trials (5 lifts or lowers per trial) constituting 115 total lift/lower cycles.

Overall, the participants exploit gravity in a similar manner to lower the load and thus little performance differences arise across trials for the lowering phase of the task. In particular, the variations in time, power and motion smoothness for the lowering phase are one-third to one-half those of the lifting phase. Results reveal that lifting time is strongly correlated with lifting power (as expected) but also correlated with motion smoothness. Thus, participants in this study who lift rapidly do so with significantly greater power using motions that simultaneously minimize motion jerk.

Declaration of interests

Conflicts of interest

None.

Acknowledgement

This material is based upon work supported by the US Army Contracting Command-APG, 435 Natick Contracting Division, Natick, MA, under contract W911QY-15-C-0053.

References

Albert, W.J., Stevenson, J.M., Costigan, P.A., 1999. Quantification of lifting technique in a manual materials handling plant. Adv. Occu. Ergon. Safety 3, 73–79.
Atkeson, C.G., Hollerbach, J.M., 1985. Kinematic features of unrestrained vertical arm movements. J. Neurosci. 5 (9), 2318–2330.
Breteler, M.D.K., Gielen, S.C.A.M., Meulenbroek, R.G.J., 2001. End-point constraints in aiming movements: effects of approach angle and speed. Biol. Cybern. 85 (1), 65–75.
Cain, S.M., McGinnis, R.S., Davidson, S.P., Vitali, R.V., Perkins, N.C., McLean, S.G., 2016. Quantifying performance and effects of load carriage during a challenging balancing task using an array of wireless inertial sensors. Gait Posture 43, 65–69.
Chen, Y.L., 2000. Optimal lifting techniques adopted by Chinese men when determining their maximum acceptable weight of lift. Am. Ind. Hygiene Assoc. J. 61 (5) 642:648.
Davidson, S.P., Cain, S.M., McGinnis, R.S., Vitali, R.V., Perkins, N.C., McLean, S.G., 2016. Quantifying warfighter performance in a target acquisition and aiming task using wireless inertial sensors. Appl. Ergon. 56, 27–33.
Duong, H.T., Suh, Y.S., 2017. Walking parameters estimation based on a wrist-mounted inertial sensor for a walker user. IEEE Sensors J. 17 (7), 2100–2108.
Faber, G.S., Kingma, I., Kuijer, P.P.F.M., van der Molen, H.F., Hoozemans, M.J.M., Frings-Dresen, M.H.W., van Dieen, J.H., 2009. Working height, block mass and one- vs. two-handed block handling: the contribution to low back and shoulder loading during masonry work. Ergonomics 52 (9), 1104–1118.
Flash, T., 1987. The control of hand equilibrium trajectories in multijoint arm movements. Biol. Cybern. 57 (4–5), 257–274.
Flash, T., Hogan, N., 1985. The coordination of arm movements – an experimentally confirmed mathematical-model. J. Neurosci. 5 (7), 1688–1703.
Freivalds, A., Chaffin, D.B., Arun, G., Kwan, S.L., 1984. A dynamic biomechanical evaluation of lifting maximum acceptable loads. J. Biomech. 17 (4), 251–262.
Hasan, Z., 1986. Optimized movement trajectories and joint stiffness in unperturbed, inertially loaded movements. Biol. Cybern. 53 (6), 373–382.
Hsiang, S.H., McGorry, R.W., 1997. Three different lifting strategies for controlling motion patterns of the external load. Ergonomics 40, 928–939.
Jean-Louis, G., Kripke, D.F., Mason, W.J., Elliott, J.A., Youngstedt, S.D., 2001. Sleep estimation from wrist movement quantified by different actigraphic modalities. J. Neurosci. Methods 105 (2), 185–191.
Johannsen, D.L., Calabro, M.A., Stewart, J., Franke, W., Rood, J.C., Welk, G.J., 2010. Accuracy of armband monitors for measuring daily energy expenditure in healthy adults. Med. Sci. Sports 42 (11), 2134–2140.
Katz, J.N., 2006. Lumbar disk disorders and low-back pain: socioeconomic factors and consequences. J. Bone Jt. Surg. 88 (2), 21–24.
King, K.W., Yoon, S.W., Perkins, N.C., Najafi, K., 2008. Wireless MEMS inertial sensor system for golf swing dynamics. Sensors and Actuators A: Physical 141, 619–630.
Kollmitzer, J., Oddsson, L., Ebenbichler, G.R., Giphart, J.E., De Luca, C.J., 2002. Postural control during lifting. J. Biomech. 35 (5), 585–594.
Krismer, K., van Tulder, M., 2007. Low pack pain (non-specific). Best Practices Res. Clin. Rheumatol. 21, 77–91.
Lee, T.H., 2015. The effects of load magnitude and lifting speed on the kinematic data of load and human posture. Int. J. Occup. Saf. Ergon. 21 (1), 55–61.
Lee, B.C., Kim, J., Chen, S., Sienko, K.H., 2012. Cell phone based balance trainer. J. Neuroeng. Rehabil. 9 (10). http://dx.doi.org/10.1186/1743-0003-9-10.
Maduri, A., Pearson, B.L., Wilson, S.E., 2008. Lumbar-pelvic range and coordination during lifting tasks. J. Electromyogr. Kinesiol. 18 (5), 807–814.
McGinnis, R.S., Perkins, N.C., 2012. Highly miniaturized, wireless inertial measurement unit for characterizing the dynamics of pitched baseballs and softballs. Sensors 12, 11933–11945.
McGinnis, R.S., Cain, S.M., Davidson, S.P., Vitali, R.V., Perkins, N.C., McLean, S.G., 2016. Quantifying the effects of load carriage and fatigue under load on sacral kinematics during countermovement jump with IMU-based method. Sports Eng. 19, 21–34.
Mitchell, K.B., Batty, J.M., Coyne, M.E., DeSimone, L.L., Bensel, C.K., 2016. Reliability Analysis of Time to Complete the Obstacle Course Portion of the Load Effects Assessment Program (LEAP). Natick TR-17/002.
Nguyen, H., Lebel, K., Boissy, P., Bogard, S., Goubault, E., Duval, C., 2017. Auto detection and segmentation of daily living activities during a timed up and go task in people with Parkinson's disease using multiple inertial sensors. J. Neuroeng. Rehabil. 14 (26). http://dx.doi.org/10.1186/s12984-017-0241-2.
Ojeda, L., Borenstein, J., 2007. Non-GPS navigation for security personnel and emergency responders. J. Navigation 60 (3), 391–407.
Rebula, J.R., Ojeda, L.V., Adamczyk, P.G., Kuo, A.D., 2013. Measurement of foot placement and its variability with inertial sensors. Gait Posture 38, 974–980.
Rogers, R.M., 2003. Applied Mathematics in Integration Navigation Systems. American Institute of Aeronautics and Astronautics.
Savage, P.G., 2002. Strapdown Analytics. Strapdown Associates, Inc., Maple Plane.
Shair, E.F., Ahmad, S.A., Marhaban, M.H., Tamrin, S.B.M., Abdullah, A.R., 2017. EMG processing measures of fatigue assessment during manual lifting. BioMed Res. Int., 3937254.
Singh, R.P., Batish, A., Singh, T.P., 2014. Determining safe limits for significant task parameters during manual lifting. Workplace Health Saf. 62 (4), 150–160.
Song, J.H., Qu, X., 2014a. Effects of age and its interaction with task parameters on lifting biomechanics. Ergonomics 57 (5), 653–668.
Song, J., Qu, X., 2014b. Age-related biomechanical differences during asymmetric lifting. Int. J. Ind. Ergon. 44, 629–635.
Song, J.H., Qu, X., Chen, C., 2015. Lifting motion simulation using a hybrid approach. Ergonomics 58 (9), 1557–1570.
Song, J.H., Qu, X., Chen, C., 2016. Simulation of lifting motions using a novel multi-objective optimization approach. Ergonomics 53, 37–47.
Uno, Y., Kawato, M., Suzuki, R., 1989. Formation and control of optimal trajectory in human multijoint arm movement – minimum torque-change model. Biol. Cybern. 61 (2), 89–101.
Xiang, Y.J., Arora, J.S., Abdel-Malek, K., 2012. 3D human lifting motion prediction with difference performance measures. Int. J. Humanoid Robotics 9 (2), 1250012.